Supporting Information

Electrocatalytic Enhancement of CO Methanation at the Metal-Electrolyte Interface Studied using In Situ X-ray Photoelectron Spectroscopy

Christoph W. Thurner [1†], Leander Haug[1†], Daniel Winkler[1†], Christoph Griesser[1], Matthias Leitner[1], Toni Moser[1], Daniel Werner[1], Marco Thaler[1], Lucas A. Scheibel[1], Thomas Götsch[2], Emilia Carbonio[2,3], Julia Kunze-Liebhäuser[1], Engelbert Portenkirchner[1], Simon Penner[1] and Bernhard Klötzer[1, *]

[1]*Institute of Physical Chemistry, University of Innsbruck, Innrain 52c, A-6020 Innsbruck, Austria*

[2]*Department of Inorganic Chemistry, Fritz-Haber Institute of the Max-Planck Society, Faradayweg 4–6, Berlin 14195, Germany*

[3]*Catalysis for Energy, Energy Materials In-situ Laboratory (EMIL), Helmholtz-Zentrum Berlin für Materialien und Energie GmbH, BESSY II, Albert-Einstein-Straße 15, 12489 Berlin, Germany*

[†] C. W. T., L. H. and D. W. contributed equally and share first authorship

[*] Corresponding Author: [E-mail: bernhard.klötzer@uibk.ac.at]

SOEC cell preparation, sample mounting, equipment and XPS data analysis

In the first step, the Pt/GDC and Ni(Cu)/8-YSZ cermet powders were synthesized. For Pt/GDC-10 (volume ratio 52:48) a wet-impregnation approach was followed. A pre-sintered (12 h, 1123 K, 5% H_2 in He) GDC-10 nanopowder ($Gd_{0.1}Ce_{0.9}O_{1.95}$, Sigma Aldrich, 99.9 %) was suspended in water. An aqueous solution of H_2PtCl_6 (Sigma Aldrich, 99.9 % trace metals basis) was added dropwise to the stirred suspension. After evaporation of the water and drying at 393 K for 5 h, the hygroscopic, red-brownish crystals were mortared and transferred into an alumina boat. The chloride-containing powder was decomposed by heating from 423 K to 573 K within 2 h in He atmosphere under the evolution of Cl_2 gas. After an oxidative (He:O_2 1:1, 873 K, 3 h) and reductive (He:H_2 5:1, 673 K, 3 h) treatment, the final powder was obtained.

For the WE a Ni(Cu)/8-YSZ cermet powder (volume ratio 1:1) was prepared as follows: An aqueous solution of Ni-nitrate ($Ni(NO_3)_2 \cdot 6H_2O$, Alfa Aesar, 99,9985 % (metal basis)) and Cu-nitrate ($Cu(NO_3)_2 \cdot 6H_2O$, Merck, 99.5 %) was added dropwise to an aqueous suspension of pre-sintered (12 h, 1123 K, 5% H_2 in He) 8-YSZ nanopowder $(ZrO_2)_{0.92}(Y_2O_3)_{0.08}$ Sigma Aldrich, 99,9 % trace metals basis). Afterwards an excess of NaOH solution (1 M) was slowly added to the stirred suspension. The precipitate was filtered, washed and dried (393 K, 72 h). The mortared powder was treated in He at 623 K for 3 h to decompose the metal hydroxides. An oxidative (He:O_2 1:1, 1123 K, 3 h) and reductive (He:H_2 5:1, 1073 K, 2 h) treatment was carried out to yield the final powder.

The cells were terminated with the respective Ni/8 YSZ or $Ni_{80}Cu_{20}$/8 YSZ cathode layer on one side and with an anode layer made from Pt and GDC-10 on the other. The contacting wires and the powders were filled and smoothed out layer by layer into a pressing-body (diameter 10 mm) according to the following layered structure: Ni-wire // Ni(Cu)/8-YSZ // 8-YSZ // K-Type thermocouple // 8-YSZ // Pt/GDC // porous Pt // Pt-wire (Figure S1, B). The stack was pressed with 50 kN/cm^2 and sintered in a He:H_2 (5:1) mixture at 1523 K for 3 h. The final cell was then mounted on the sample holder and connected electrically (Figure S1, C). A scheme of the sample holder and the surrounding setup is shown in Figure S1, panel A. The embedded thermocouple inside the electrolyte layer allows for power control of an infrared heating laser (Figure S1,A). For the electrochemical experiments a BioLogic potentiostat was used. Product detection was achieved by on-line MS (Pfeiffer) directly attached to the NAP-XPS chamber. To investigate the electrochemically active zone within the Ni(Cu)/8-YSZ layer with a maximum of accessible TPD sites (i.e., the

interfacial region between the working electrode and the electrolyte), a small concave pit was milled into the mounted cell (Figure S1, A). The XPS data analysis was performed using the CasaXPS software, version 2.3.24 PR1.0 (Casa Software Ltd.). Fitting parameters were kept constant and originate from literature [1].

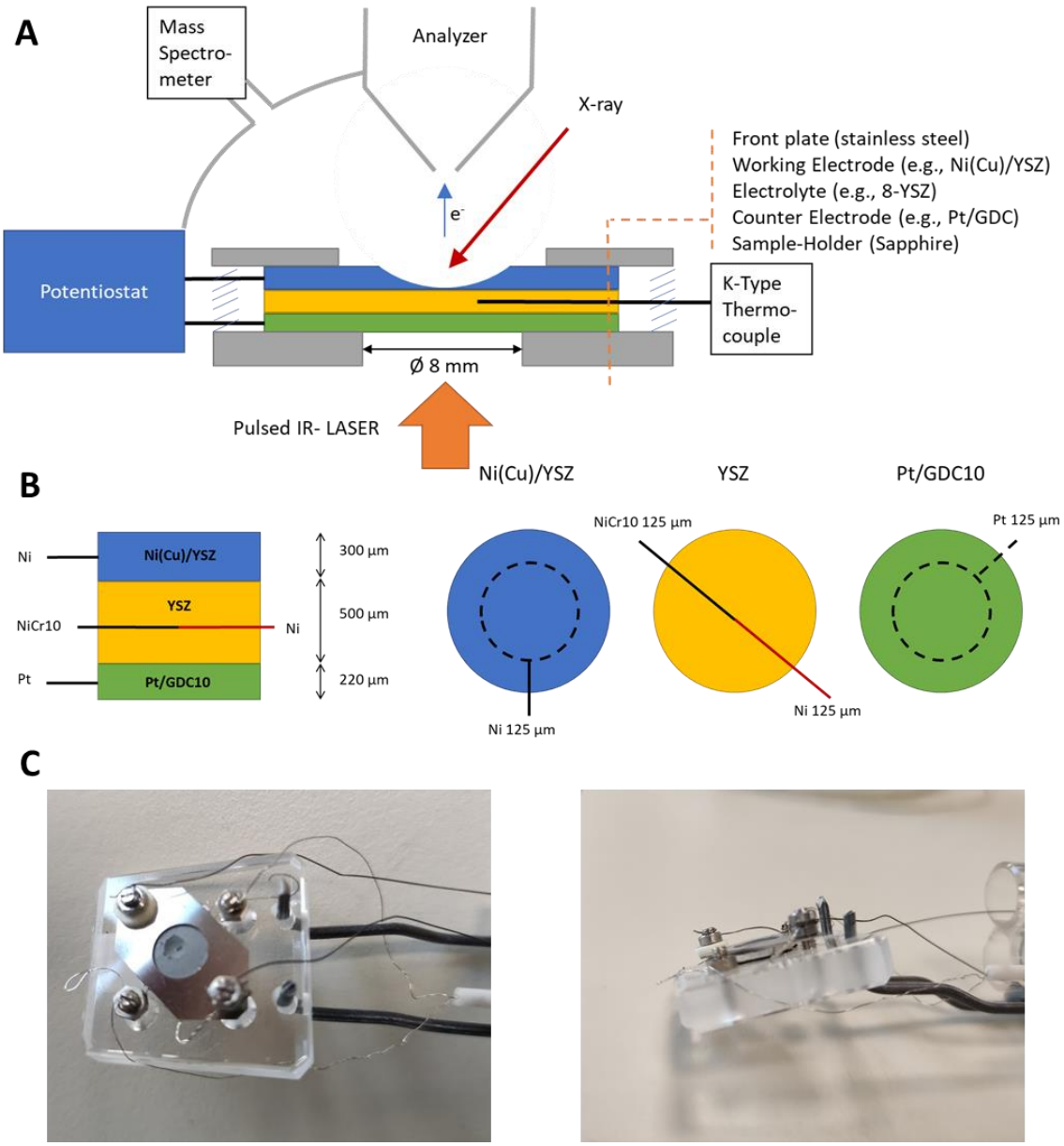

Figure S1. Panel A displays a scheme of the setup and the sample holder. In panel B, the layered structure of the cell is illustrated. Circular Ni and Pt wires with 125 µm thickness each were embedded in the respective electrode layers to ensure optimum electrical contact, and spot-welded 125 µm Ni and NiCr thermocouple wires were embedded in the 8-YSZ electrolyte layer. A photograph of the sample holder with mounted cell is shown in panel C.

XPS comparison of Ni/8-YSZ vs. $Ni_{80}Cu_{20}$/8-YSZ upon carbon accumulation

Figure S2 confirms that carbon is accumulated via the TPB onto the porous cermet surface by presenting the qualitative visible decrease of the integral peak area of the Cu 2p, Ni 2p and Zr 3d region and the increase of the C 1s region. The top row shows the initial status before carbon growth (black traces), while the bottom row indicates the situation after electrochemically induced carbon growth in CO atmosphere. To prove if any oxidic state is present in the CuNi alloy, a spectrum of the Cu 2p and Ni 2p region recorded under H_2 atmosphere (0.5 mbar, brown trace, ensuring the metallic state of the alloy) was subtracted from the normalized experimental data (black trace). The residual (grey trace) shows no visible Cu(II) satellite feature in Cu 2p region and no oxidic species in the Ni 2p region confirming the purely metallic state of the alloy in CO atmosphere. The peak positions for a $Ni_{80}Cu_{20}$ alloy (Cu $2p_{3/2}$ = 932.6 eV and Ni $2p_{3/2}$ = 852.7 eV) are taken from [2].

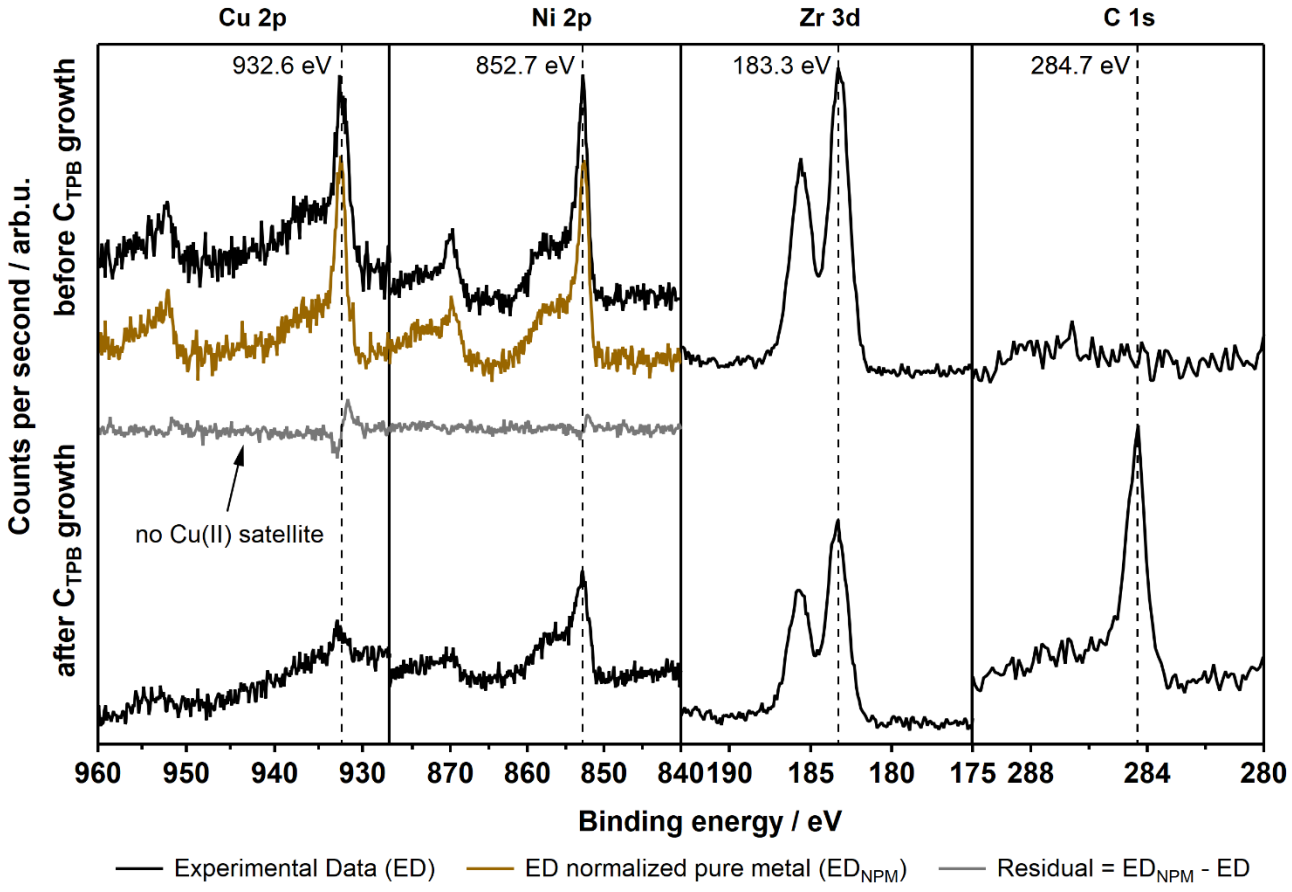

Figure S2. XP-spectra of the Cu2p, Ni2p, Zr3d and C1s region are exemplary shown for the $Ni_{80}Cu_{20}$/8-YSZ electrode before (top row) and after (bottom row) electrochemically induced carbon growth recorded in CO atmosphere.

Thermodynamic promotion of CH_4 formation

Figure S3 supports the argumentation of an increase in CH_4 partial pressure and a decrease in Gibbs free energy for methane formation due to an increase of carbon activity, which can be achieved by cathodic electrochemical polarization.

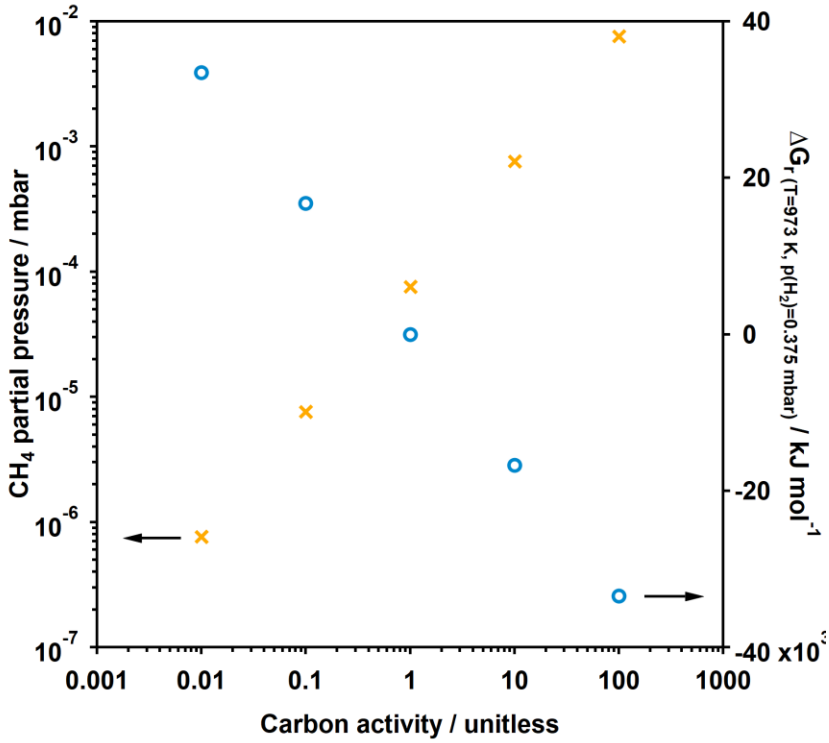

Figure S3. The figure compares the thermodynamic results of reaction 6 for a given set of parameters ($p(H_2)$ = 0.375 mbar and T = 973 K). The methane partial pressure (orange crosses) and the Gibbs free energy (blue circles) are plotted as a function of carbon activity.

QMS data analysis and Cyclovoltammetry I vs. E curves

From the experimental data we figured out that there is a clear dependence of applied potential and product detection via mass spectroscopy. We observe this dependence not only for the *m/z*=15 signal, but also for example for *m/z*=44 CO_2 (if CO is oxidized) or *m/z*=18 H_2O (if H_2 is oxidized; both not shown). Based on several experiments the delay time between the maximum applied potential during the CV and the QMS signal peak was found to be 90 s. The

delay-time corrected data are shown in Fig. 3 in the main paper. The I vs. E curves which corresponds to the data presented in Fig 3. (main paper) are shown in Figure S4.

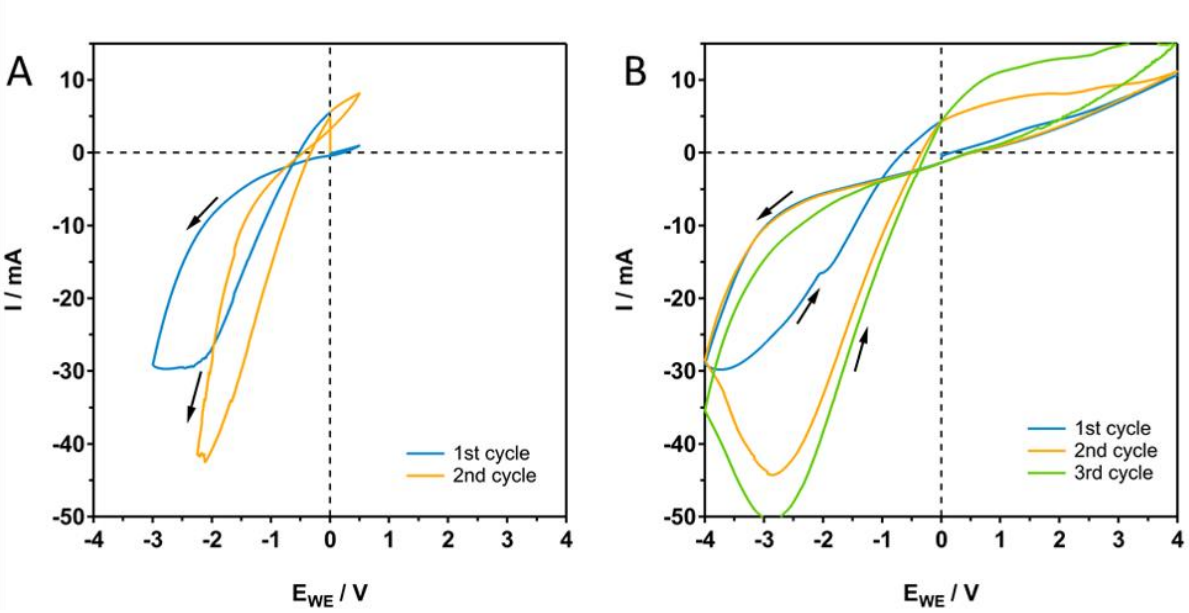

Figure S4. Corresponding I vs. E curves to the data shown in Figure 3 in the main paper. A: Cathodic polarization of $Ni_{80}Cu_{20}$/8-YSZ and B: cathodic and anodic polarization of $Ni_{80}Cu_{20}$/8-YSZ

Operando XPS comparison of Ni/8-YSZ vs. $Ni_{80}Cu_{20}$/8-YSZ in CO/H_2 atmosphere

Figure S5 shows an operando experiment comparing Ni/8-YSZ vs. $Ni_{80}Cu_{20}$/8-YSZ under chronoamperometric cathodic polarization of the WE in syngas atmosphere. While applying a bias of -1.00 V for Ni/8-YSZ and -1.25 V for $Ni_{80}Cu_{20}$/8-YSZ, the MS detects the additional methane product formation on-line and XPS validates the absence and presence of C_{TPB} for each type of electrode. The data support the statement in the main paper that the electrocatalytic enhancement effect on Ni/8-YZS vs. $Ni_{80}Cu_{20}$/8-YSZ is proven qualitatively, but hard to distinguish quantitatively (panels B and D).

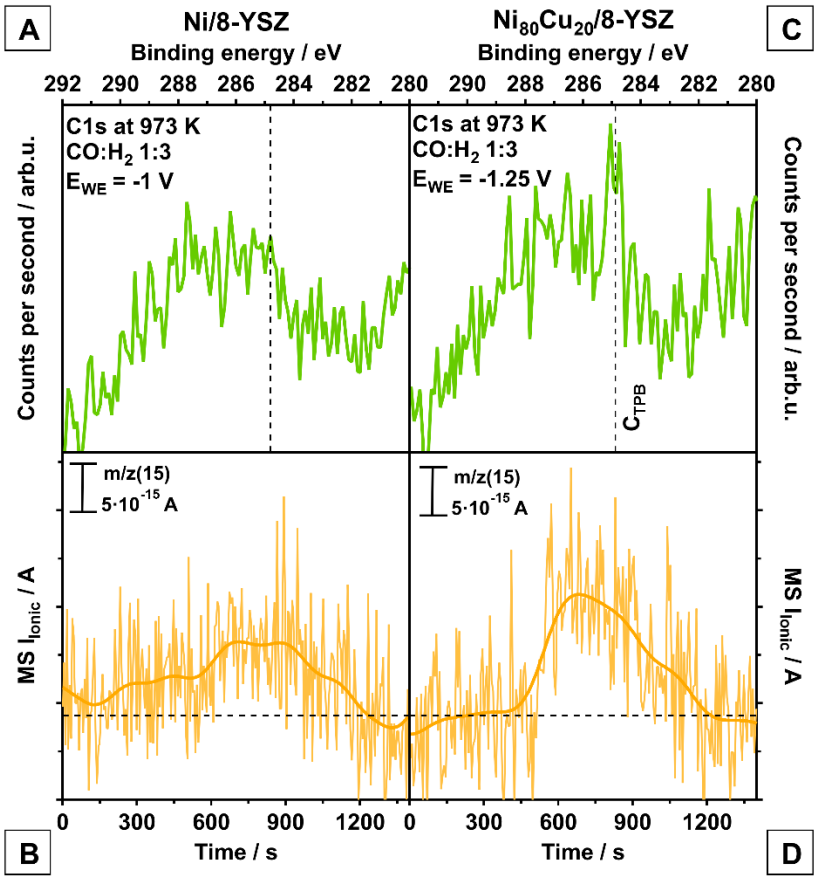

Figure S5. Operando XPS on Ni/8-YSZ (left side) vs. $Ni_{80}Cu_{20}$/8-YSZ (right side). Panels A and C show the C 1s XP-spectra (green traces) recorded at 973 K in 0.500 mbar $CO:H_2$ = 1:3 atmosphere, while polarizations of -1.00 V (Ni/8-YSZ) and -1.25 V ($Ni_{80}Cu_{20}$/8-YSZ) were applied to the WE. Panels B and D (light orange traces, raw and smoothed experimental data) show the electrochemically promoted excess methane formation caused by the chronoamperometric cathodic polarization.

To confirm the anticipated metallic state of Ni/Cu under the applied reductive conditions ($CO:H_2$ = 1:3 we exemplary show) in Figure S6 the Cu 2p and Ni 2p XP-spectra of the $Ni_{80}Cu_{20}$/8-YSZ electrode. Figure S6 further compares a XP-spectra series recorded at OCP and at -1.25 V (same experiment as shown in Figure S5). In addition to the metals, the O 1s and C 1s XP-spectra for both potentials are shown. The C 1s data for E_{WE}=-1.25 V is the same as in Fig. S5, C. To prove if any oxidic state is present in the CuNi alloy, a spectrum of the Cu 2p and Ni 2p region recorded under H_2 atmosphere (0.5 mbar, brown trace, ensuring the metallic state of the alloy) was subtracted from the normalized experimental data (black trace). The residual (grey trace) shows no visible Cu(II) satellite feature in the

Cu 2p region and no oxidic species in the Ni 2p region confirming the pure metallic state of the alloy in CO:H_2 atmosphere. The weak feature in the oxidic Ni 2p region thus indicates a minor if at all oxidic contribution in the pure-metal spectrum recorded under H_2 (arrow). The peak positions for a $Ni_{80}Cu_{20}$ alloy (Cu $2p_{3/2}$ = 932.6 eV and Ni $2p_{3/2}$ = 852.7 eV) are taken from a XPS study of Kleiman et al. on NiCu alloys [2]. The Ni/Cu ratio of 3.08 at OCP stays the same under polarization (3.07).

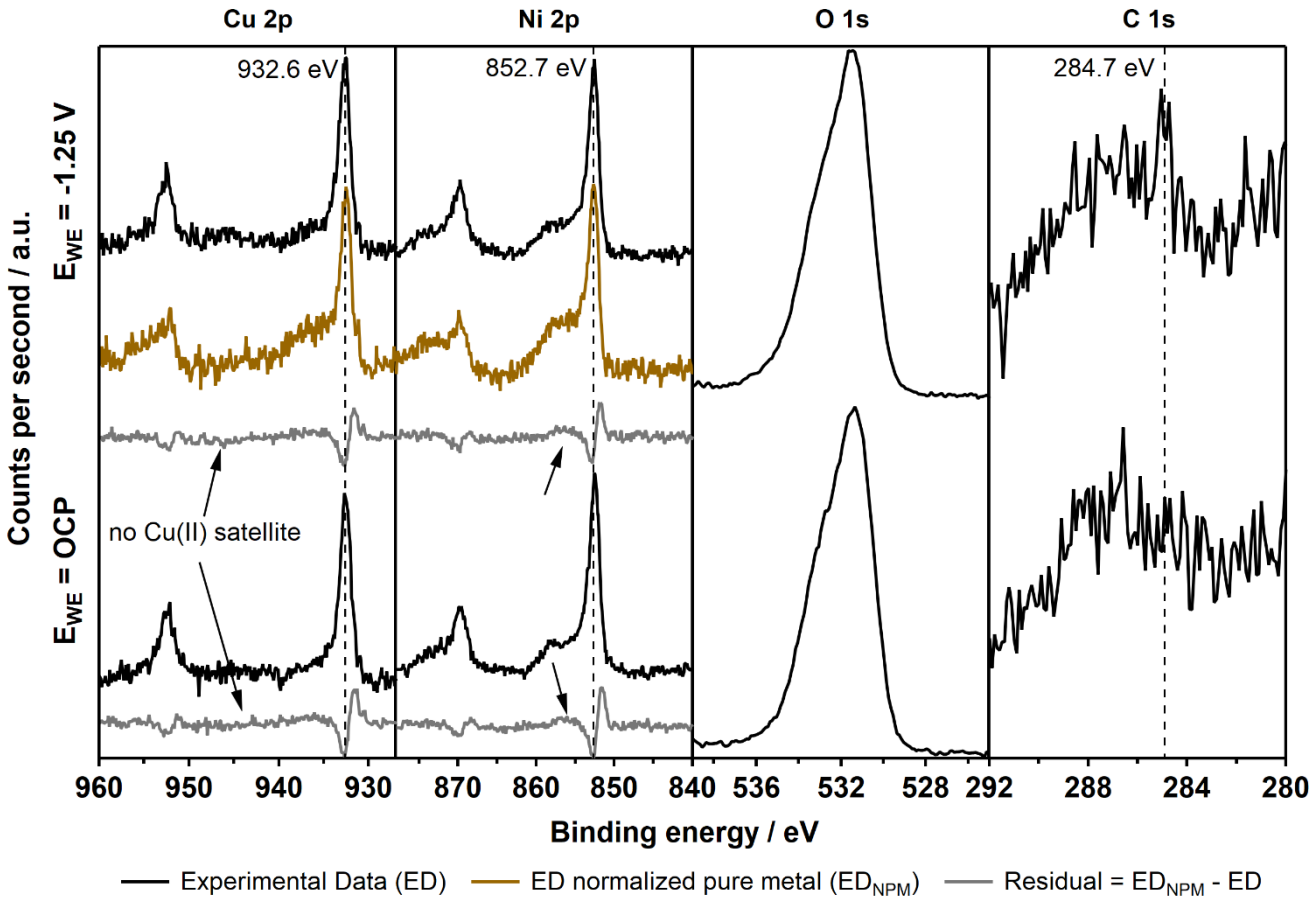

Figure S6. XP-spectra of the Cu 2p, Ni 2p, O 1s and C 1s region as well as an Auger spectrum of the Cu LMM region are exemplary shown for the $Ni_{80}Cu_{20}$/8-YSZ electrode under OCP (bottom row) and under polarization (E_{WE} = -1.25 V, top row) recorded in CO:H_2=1:3 atmosphere.

To unravel the presence of a Cu(I) state on the electrode surface we fitted Auger spectra of the Cu LMM region recorded together with the experimental data shown in Figure S6 (same conditions). Figure S7 shown the Cu LMM Auger data and the results of the applied fitting routine according to Biesinger [3]. In the top and bottom spectra (i.e., under H_2 or CO:H_2 and OCP respectively) barely any Cu(I) state appears as a consequence of the fitting procedure.

However, under an applied voltage of -1.25 V the contribution of Cu(I) increases. This observation may indicate some electrochemically induced surface oxidic species, but due to the noisy spectrum and fast kinetics at 973 K this result is not reliable and could be an artefact. The KE of 918.3 eV for a $Ni_{80}Cu_{20}$ alloy was taken from literature [2].

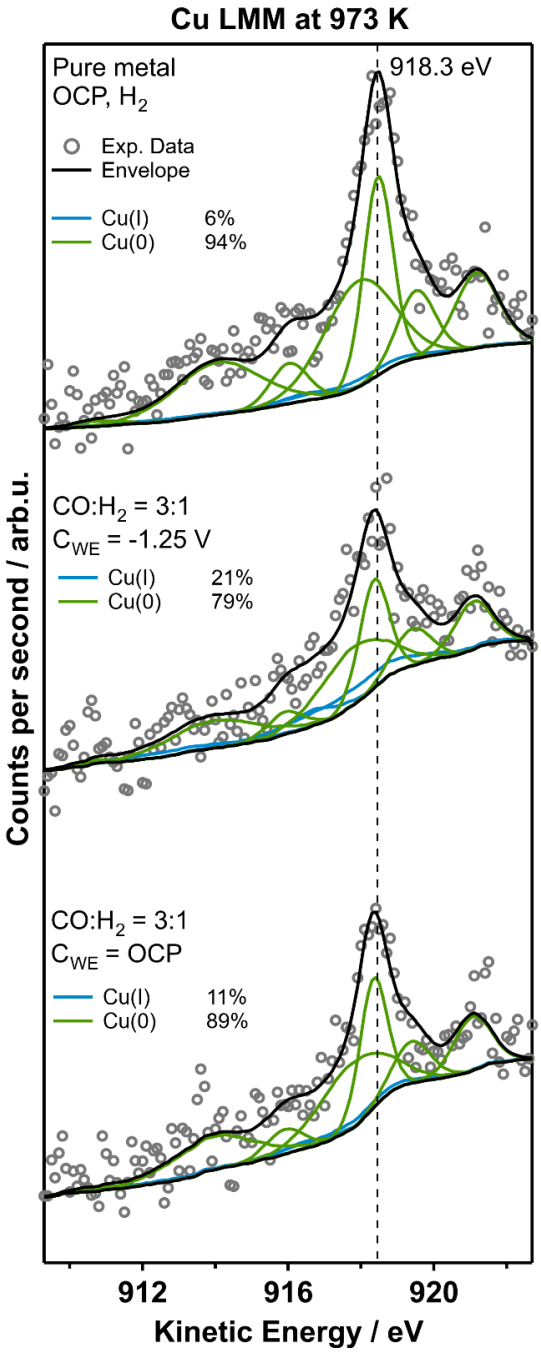

Figure S7. Auger spectra of the Cu LMM region recorded under pure H_2 0.5 mbar (top), under CO:H_2 3:1 0.5 mbar and Ewe of -1.25 V (model) and under CO:H_2 3:1 0.5 mbar and OCP (bottom). The fits and evaluation of the Cu(0) and Cu(I) state correspond to a routine published by Biesinger [3].

References:

1. Biesinger, M.C. Accessing the robustness of adventitious carbon for charge referencing (correction) purposes in XPS analysis: Insights from a multi-user facility data review. *Appl. Surf. Sci.* **2022**, *597*, 153681, doi:10.1016/j.apsusc.2022.153681.
2. Barbieri, P.F.; de Siervo, A.; Carazzolle, M.F.; Landers, R.; Kleiman, G.G. XPS and XAES study of Ag–Pd and Cu–Ni alloys: spectra, shifts and electronic structure information. *J. Electron. Spectrosc. Relat. Phenom.* **2004**, *135*, 113-118, doi:10.1016/j.elspec.2004.02.121.
3. Biesinger, M.C. Advanced analysis of copper X-ray photoelectron spectra. *Surf. Interface Anal.* **2017**, *49*, 1325-1334, doi:10.1002/sia.6239.